Structure of the myosin head in solution and the effect of light chain 2 removal

Manuel Garrigos,* Simon Mallam,‡ Patrice Vachette,§ and Joan Bordas||

*Département de Biologie, Service de Biophysique, CEN-Saclay 91191 Gif-sur-Yvette Cedex, France; ‡Centre for Energy Research and Training, Ahmadu Bello University, Zaria, Nigeria; §Laboratoire pour l'Utilisation du Rayonnement Electromagnétique, Bâtiment 209d, Université Paris-Sud, 91405 Orsay, France; and ||Daresbury Laboratory, Warrington WA4 4AD, England

ABSTRACT Structural properties of rabbit skeletal myosin head (S1) and the influence of the DTNB light chain (LC2) on the size and shape of myosin heads in solution were investigated by small angle x-ray scattering. The LC2 deficient myosin head, S1 (−LC2), and the S1 containing LC2 light chain, S1 (+LC2) were studied in parallel. The respective values of the radius of gyration were found to be (40.2 ± 0.5) Å and (46.7 ± 1) Å, while the maximum dimension was (190 ± 15) Å for both species. The large difference between the two R_g values suggest that LC2 is located close to one extremity of the myosin head, in agreement with most electron microscopy observations. All models derived from the x-ray scattering pattern of the native myosin head share a common overall morphology, showing two main regions, an asymmetric globular portion which tapers smoothly into a thinner domain of roughly equivalent length making an angle of ~60°, with a contour length of ~210 Å.

INTRODUCTION

Myosin appears morphologically as two globular domains (heads) attached to a long fibrous tail (Slayter and Lowey, 1967). Biochemically, the myosin molecule is a hexamer comprising two heavy chains of molecular weight 220,000 and four light chains of molecular weight in the range 17,000 to 22,000 belonging to two different classes called the alkali (LC1 and LC3) and DTNB (LC2) light chains. The carboxyl-terminal part (about 1,100 amino acids) of each heavy chain forms an α-helical coiled-coil rod (tail). The amino-terminal part (~850 amino acids) of each heavy chain together with two light chains (one of each class) form the globular domain of the myosin molecule (head). Functionally, the head region carries the ATPase and actin binding sites. Moreover, it has been shown that the isolated myosin head (myosin subfragment 1 or S1) is sufficient to drive the sliding movement of actin filaments (Toyoshima et al., 1987). It follows that S1 size and shape are essential parameters for understanding any model of muscular contraction at the molecular level. They are also absolute requirements for a detailed interpretation of muscle x-ray diffraction experiments and three-dimensional reconstructions (Squire, 1981, 1987).

As far as the shape of S1 is concerned, the results obtained from a variety of techniques, mainly hydrodynamic methods together with small angle x-ray scattering and electron microscopy, are consistent with the general picture of a fairly anisometric shape for S1. Three-dimensional reconstruction applied to tannic acid-stained thin sections of embedded chicken myosin S1 crystals reveals a tadpole like shape for S1 (Winkelmann et al., 1985, 1991). This shape is roughly similar to the head shape observed by negative staining or rotary shadowing which has been defined by electron microscopists as a 'comma,' a 'banana', or a 'pear' with the narrow end being part of the junction with the tail. These images mainly emphasize the curved appearance of the particle when observed by electron microscopy.

In contrast with this consensus view about the shape of S1, the size of the head is still a matter of debate. Estimates of the dimensions of S1 were derived from electron micrographs of native thick filaments (Knight and Trinick, 1984), of S1-decorated actin filaments (Seymour and O'Brien, 1985; Milligan and Flicker, 1987; Kajiyama, 1988), of isolated myosin molecule (Elliott and Offer, 1978; Takahashi, 1978; Walker et al., 1985), isolated S1 (Winkelmann and Lowey, 1986; Vibert, 1988) as well as of S1 crystals (Winkelmann et al., 1985, 1991). The contour length (L_{max}) of S1 was found to be in the range 160 Å < L_{max} < 220 Å. The lower value has been determined by electron microscopy on S1 crystals but because two molecules of S1 were found to overlap partially in the crystal unit, this value can only be considered as a lowest limit. However, even this lowest limit is significantly larger than the D_{max} value of 120 Å obtained by small angle x-ray scattering of S1 solutions (Mendelson et al., 1980). This discrepancy has been discussed by Craig (Craig et al., 1986) and mainly attributed to intrinsic artefacts or limitations of the techniques used. We have performed x-ray solution scattering experiments on S1 and obtained structural parameters in agreement with electron microscopy observations.

The global structure of S1 has also been shown to be very sensitive to the presence of LC2; removal of this light chain from myosin results in a loss of the elongated pear-shaped appearance to yield instead shorter, more

Address correspondence to M. Garrigos.

Abbreviations used: LC2, the phosphorylatable light chain from vertebrate myosin also called DTNB light chain because it is dissociated from myosin heavy chain with 5,5-dithiobis-(2-nitrobenzoate); S1 (+LC2) or S1 (−LC2), skeletal myosin subfragment 1 with or without light chain 2, respectively; DTT, dithiothreitol; MBS, m-maleimidobenzoyl-*N*-hydroxysuccinimide ester; HPSEC, high performance size exclusion chromatography.

0006-3495/92/12/1462/09 $2.00

rounded heads (Winkelmann and Lowey, 1986). In this report, we have also investigated whether the removal of LC2 influences the global conformation of rabbit skeletal S1 in solution.

A preliminary account of this work was presented earlier in abstract form (Garrigos and Vachette, 1989).

MATERIALS AND METHODS

Chemicals

Nα-*p*-Tosyl-L-lysine chloromethyl ketone treated α-chymotrypsin was purchased from Sigma Chemical Co., St. Louis, MO). All other chemicals were of the highest analytical grade.

Protein preparation

Rabbit skeletal myosin from back and hind leg fast muscles was prepared according to Perry (1955) as modified by d'Albis et al. (1979) and stored in 50% glycerol at −20°C. S1 (−LC2) and S1 (+LC2) were obtained, respectively, after chymotryptic or papain digestion of myosin filaments as described by Margossian and Lowey (1982). Both subfragments were purified by high performance gel filtration chromatography at room temperature using a (0.75 × 30 cm) TSK 3000 SW column equilibrated with buffer A: Imidazole-HCl 50 mM pH 7.0, NaCl 100 mM, DTT 2 mM, $MgCl_2$ 2 mM. Each subfragment 1 was eluted ~7 min after sample injection onto the column. The column-purified subfragments were either used just after being chromatographed or dialyzed against 4 mM ammonium acetate pH 7.0, 1 mM DTT at 5°C. In the latter case 4 mg of sucrose were added for each milligram of S1 and the protein solution was frozen and lyophilized (Margossian and Lowey, 1982). The lyophilized S1 was stored as a freeze-dried powder at −20°C. When freeze-dried S1 were used, samples containing ~18 mg of protein were dissolved in 200 μl of buffer A. Then any undissolved material was removed by filtration through a 0.22 μm Millex GV_4 filter (Millipore). Finally, S1 sample was applied to a TSK 3000 SW column equilibrated with the same buffer in order to eliminate any aggregated material (Fig. 1). Typically, ten 100-μl fractions were collected from the major peak, corresponding to the shaded area in Fig. 1. Each fraction was rechromatographed and only those whose homogeneity, as determined by the peak integrator, was found to be better than 99% were examined by x-ray scattering (Fig. 1). The chemical homogeneity of S1 (−LC2) and S1 (+LC2) subfragments as well as their light chain composition were analyzed by sodium dodecyl sulfate gel electrophoresis in 12% polyacrylamide slab gels (Fig. 1). Protein concentration of every HPSEC fraction was determined by HPSEC using a Spectra-Physics integrator previously calibrated with S1 solutions the concentrations of which (mg × ml^{-1}) were measured spectrophotometrically using the following extinction coefficients: $\epsilon^{0.1\%}_{280nm} = 0.75\ cm^{-1}$ for S1 (−LC2), and 0.83 cm^{-1} for S1 (+LC2) (Margossian and Lowey, 1982).

X-ray scattering experiments

Data were recorded on the small angle scattering instrument D24 at the LURE synchrotron facility in Orsay (Depautex et al., 1987). The storage ring D.C.I. was operated at 1.85 Gev and 250–300 mA. The x-ray beam has a cross-section of 0.5 × 2.0 mm at the sample level and 0.5 × 1.0 mm at the detector level. A linear position sensitive detector with delay-line readout was used with a 3 mm wide entrance window. The data acquisition system, developed at the EMBL (Heidelberg and Hamburg) has already been described (Bordas et al., 1980). The scattering parameter is $s = 2 \sin \theta/\lambda$, where 2θ is the scattering angle, and the wavelength $\lambda = 1.608$ Å (K-edge of cobalt). The small-angle data (s-range from 1.1×10^{-3} $Å^{-1}$ to 1.2×10^{-2} $Å^{-1}$) were recorded with a sample-to-detector distance of 1,315 mm with a corresponding channel width of $ds = 1.003 \times 10^{-4}$ $Å^{-1}$/channel. The counting time was 4 × 200 s. For the wide-angle pattern (s-range from 2.7×10^{-3} $Å^{-1}$ to 6.7×10^{-2} $Å^{-1}$), the distance was 815 mm with a channel width of $ds = 1.796 \times 10^{-4}$ $Å^{-1}$/channel, and the counting time was 15 × 200 s. All solutions were studied at room temperature in the same flattened quartz capillary 0.9 mm thick, rinsed between two successive samples while being kept in position. Every single 200-s frame was checked for possible radiation damage before averaging. Indeed, some slight but significant differences between successive frames were detected after ~600 s x-ray exposure. Thus, the protein solution in the beam was renewed after 400 s of exposure. All samples were rechromatographed immediately after x-ray exposure as an extra check of solution homogeneity.

The background scattering from slits, residual air path, capillary tube and buffer, was measured, normalized and subtracted from the scattering of the protein solution. The radius of gyration and the intensity at the origin were obtained from a linear regression on a Guinier plot ($\ln [I(s)] = f(s^2)$) of the background-corrected intensities (Guinier and Fournet, 1955; Luzzati, 1960). A solution of 6.7 mg/ml aspartate transcarbamylase (ATCase) from *E. coli* was used as a reference to derive a value for the relative molecular weights of both S1 subfragments. ATCase is a stable protein which presents no detectable interactions in solutions of low to moderate concentration (<15 mg/ml), the scattering curve of which shows a very extended Guinier region. It has a molecular weight of 306 kD and a partial specific volume of 0.739 $cm^3 \times g^{-1}$ (Hoover et al., 1983; Moody et al., 1979).

On one data set, the distance distribution function $p(r)$ obtained by Fourier transform of the scattering curve has been calculated using three different programs: a conventional sine transform after extrapolation to zero angle (Guinier extrapolation) and to infinity (Porod law), the program ITP for Indirect Fourier Transform by Glatter (Glatter, 1977) and the program GNOM for small angle scattering data analysis by Svergun et al. (1988) in its latest version including error propagation by a Monte-Carlo method. The resulting distance distribution curves did not show any significant differences. All subsequent calculations were made using the interactive version of the program GNOM. Calculations were made using different cutoff positions between 0.031 and 0.067 $Å^{-1}$ without any significant change.

Model calculations

The model calculations were carried out using the programme DALAI (E. Pantos, J. West, and J. Bordas, unpublished data) installed on an Ardent-Titan super minicomputer and on a Convex at Daresbury Laboratory. The algorithms are based on calculating x-ray solution scattering patterns using Debye's formula. The initial model is built from a series of spheres of a given diameter and density contained within a cylinder of maximal outer dimensions defined by the user, in our case 70 Å diameter and 230 Å in length. The initial iterations are based on all combinations between groups of spheres in which densities of either zero and one are permutated. Usually a good set of approximate models are obtained quite quickly. Having defined the common characteristics of these models a new starting model with refined dimensions and a larger number of smaller spheres (i.e., higher resolution) is built and now all combinations of spheres with density values either zero or one within the envelope are considered and the corresponding scattering patterns are calculated. The quality of the fit is determined in any iteration by calculating the residuals between the logarithms of the experimental and calculated scattered intensities. The program returns all generated models whose residuals are below a user given value (e.g., less than ±5%, as shown in the inset of Fig. 5). Any of these "generic" models can then be used for further refinement if wished. Naturally, the quality of the fit will depend on the number of spheres of ever smaller diameters used in the approximation (i.e., the resolution of the model is improved). In this case the final model comprises of 283 spheres, with a radius of 5 Å each.

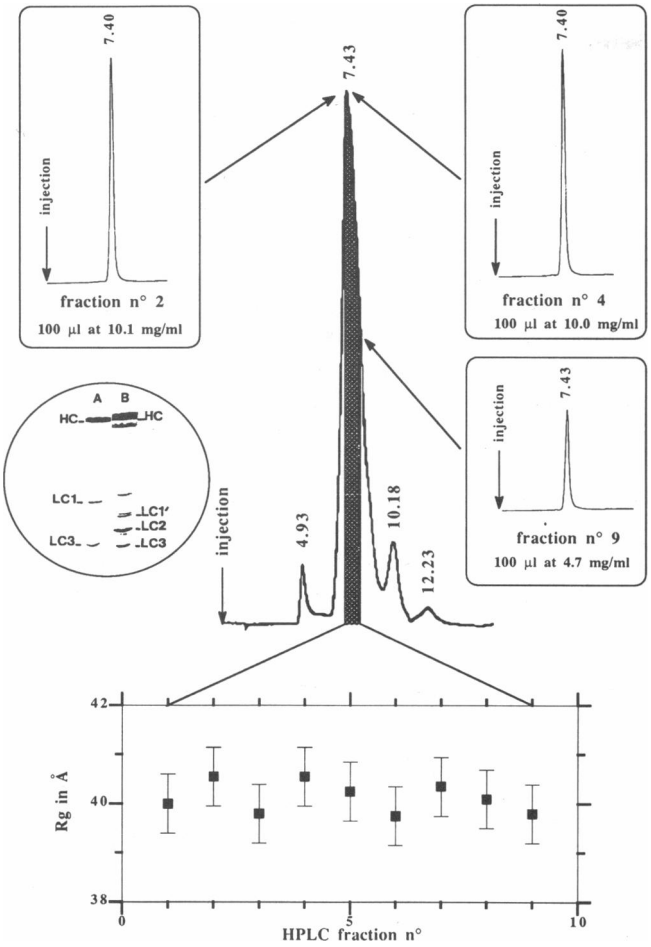

FIGURE 1 Sample purification and characterization. The center of this composite figure shows the SEC profile of crude S1 (−LC2). The shaded area corresponds to the fractions used for x-ray experiments. The three panels show the SEC profile of three individual fractions the approximate position of which is indicated by the arrows pointing towards the main peak. The bottom frame shows the value of the radius of gyration as a function of the fraction number. Inside the circle, SDS PAGE patterns: (*A*) S1 (−LC2); (*B*) S1 (+LC2). See Materials and Methods for experimental conditions.

RESULTS

As shown in Fig. 1, light chain composition of both proteolytic S1 fragments after size exclusion chromatography (SEC) was characterized by SDS gel electrophoresis. Characteristic patterns were obtained from both S1 fragments: the expected complement of light chains was observed in each case. The size homogeneity of each S1 fraction collected from the central peak (*shaded area* in Fig. 1) in view of SAXS experiments was directly ascertained by analytical SEC. As illustrated for S1 (−LC2) all profiles demonstrated the absence of any detectable amount of aggregated material (see the three panels in Fig. 1). Then, the radius of gyration was determined for every single fraction by SAXS measurements. The concentration of the collected fractions allowed direct measurements with no need for any further concentration step (see Fig. 1). They ranged from 5 to 10 mg/ml for the chymotryptic (S1 (−LC2)) myosin fragment, 8 to 14 mg/ml for the papain (S1 (+LC2)) fragment. Guinier plots are linear over the angular range $0.26 < 2\pi s R_g < 1.39$ (S1 (−LC2)) and $0.30 < 2\pi s R_g < 1.35$ (S1 (+LC2)). The R_g values are (40.2 ± 0.5) Å and (46.7 ± 1) Å for S1 (−LC2) and S1 (+LC2), respectively. They are shown in Fig. 2 while the values of the radii of gyration are plotted in the insets as a function of protein concentration. The values for S1 (−LC2) are also plotted as a function of the fraction number at the bottom of Fig. 1. In this last plot, we observe no significant differences in the R_g values among the nine fractions studied, further supporting the absence of any size heterogeneity. R_g values of both S1 preparations do not show either any significant concentration dependence in the concentration range studied. Using ATCase as a standard, the values of the molecular weight of the two fragments derived from the intensity at the origin agreed within 15% with the corresponding value derived from the amino-acid sequence (Tong and Elzinga, 1990).

Data at wider angles were recorded using concentrated solutions of S1 (+LC2) (55 mg/ml) and S1 (−LC2)

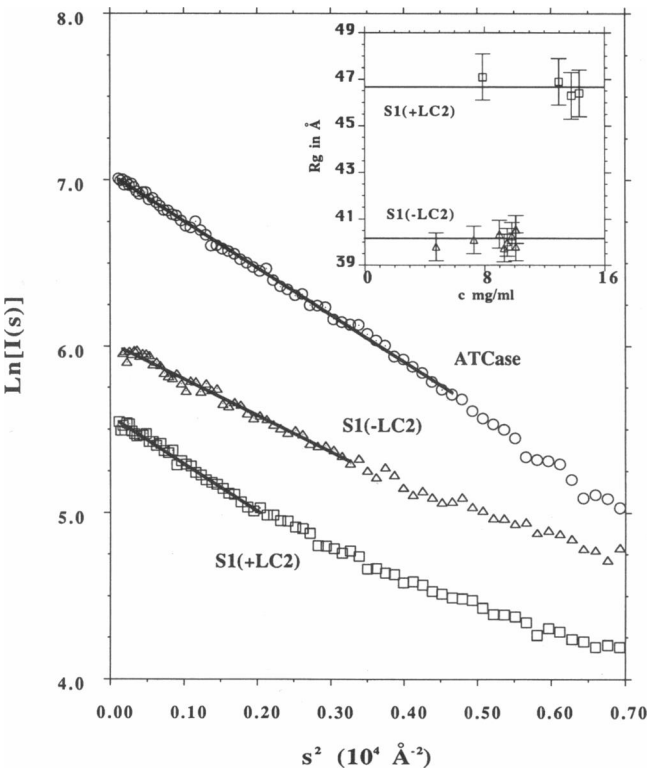

FIGURE 2 Guinier plots. Uncorrected experimental data, after background subtraction. From top to bottom: ATCase, S1 (−LC2), S1 (+LC2). The two curves have been arbitrarily shifted along the vertical axis for the sake of clarity. The thick straight line drawn through the innermost part of each data set represents the least-square linear fit to the data in the Guinier region whose slope yields the R_g values. (*Inset*) radii of gyration vs. protein concentration. See Materials and Methods for experimental conditions.

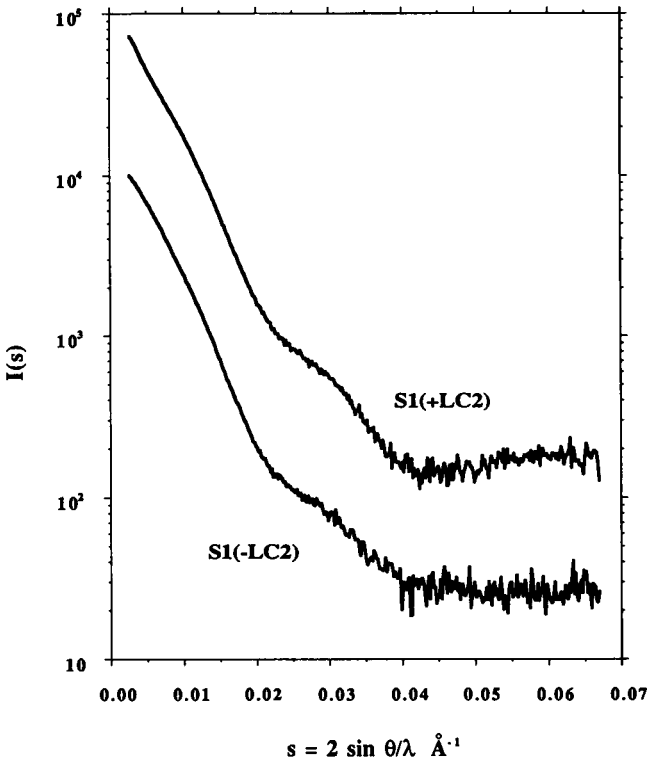

FIGURE 3 Wide-angle scattering curves. Uncorrected experimental data points after background subtraction. (*Top curve*) S1 (+LC2); (*bottom curve*) S1 (−LC2). The two curves have been arbitrarily shifted along the vertical axis for the sake of clarity. See Materials and Methods for experimental conditions.

(106 mg/ml). The two curves are plotted in Fig. 3 after background subtraction. A shoulder is clearly visible on both spectra at 0.029 $Å^{-1}$. No aggregation was detected, even at the higher concentration used; on the contrary, the only noticeable effect is a slight downward curvature in the Guinier region probably due to repulsive interactions between particules. These will help to ensure monodispersity even in nonideal solutions. Each of these curves was joined, after proper scaling, to a small angle scattering curve to give a complete pattern. Distance distribution functions were derived by Fourier transform (Fig. 4). The maximal chord D_{max} has a value of (190 ± 15) Å for both S1 (+LC2) and S1 (−LC2). The two curves show a maximum at about 35 Å regardless of the presence or absence of LC2 while differences are mainly located between 80 and 170 Å.

A comparison between the experimentally determined x-ray solution scattering pattern for S1 (+LC2) with the best model calculation is shown in Fig. 5. Morphologically, this model of the native myosin head shows two main regions, a globular portion and a thinner domain of roughly equivalent length making an angle of 60° with an overall length of ~210 Å (Fig. 6). More precisely, different regions of the scattering curve are more sensitive to distinct structural features of the model. In order to fit the low angle inflection (at 0.005 $Å^{-1}$) while achieving a reasonable agreement in the Guinier region it is necessary to have a length to width ratio of between 4 and 5, while locating most of the mass on the globular portion at the tip of the head. The fit to the Guinier region was later refined by varying the angle between the globular and the thinner parts. This had the twofold aim of improving the fit in the Guinier region while introducing an amount of curvature in the shape, a feature encountered in most electron microscopy observations. Calculations were performed using four values of the angle between 0° (straight model) and 90°. Four curves are shown on Fig. 7 together with the experimental curve for S1 (+LC2). The radii of gyration varied from 48.8 Å down to 42.9 Å. Angles compatible with our experimental value of 46.7 ± 1 Å were restricted to the range 40° to 70° as shown in the inset to Fig. 7. The asymmetric appearance of the globular end portion, as shown in the two orthogonal views displayed in Fig. 6, is required to reproduce the experimental decay of intensity in the region between 0.005 and 0.02 $Å^{-1}$. Finally, to fit the shoulder in between 0.025 and 0.045 $Å^{-1}$ it is necessary for the head to taper smoothly towards the thinner end (Fig. 6).

In the case of S1 (−LC2), simple removal of mass failed to yield a fit to the x-ray scattering data of equivalent quality. To model the absence of the shoulder at

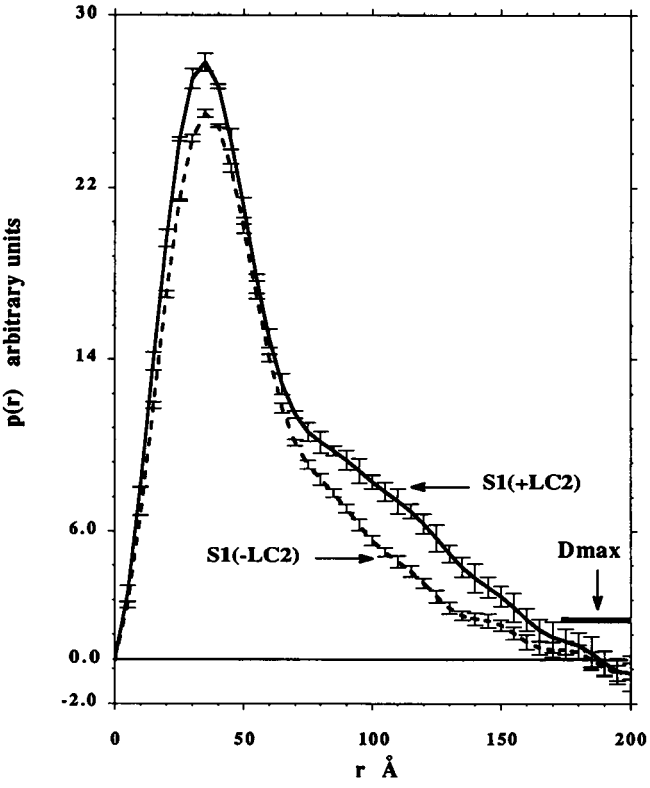

FIGURE 4 Distance distribution functions. (*Broken line*) S1 (+LC2); (*solid line*) S1 (−LC2) with associated error bars. The integral of the two curves, derived from the experimental data as explained in Materials and Methods, have been scaled to molecular weight.

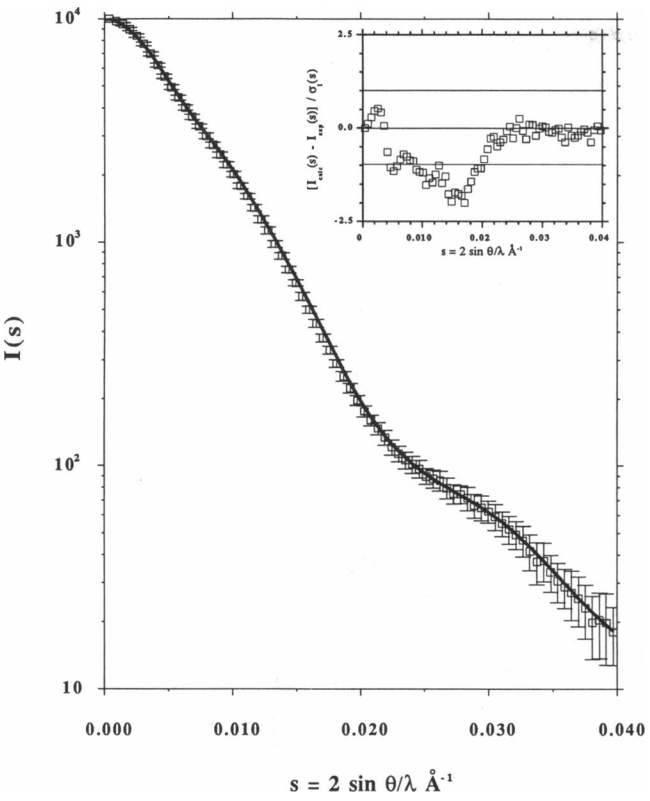

FIGURE 5 Model fitting. Comparison of the experimental x-ray scattering intensities of myosin S1 (+LC2) (*squares*) with their associated error bars with the intensities yielded by the model shown in Fig. 6 (*line*). The inset shows the residuals between these two curves (experimental − calculated) divided by the corresponding experimental uncertainties σ_I.

0.005 $Å^{-1}$, while fitting the data out to 0.025 $Å^{-1}$, it is necessary to remove mass from the model and simultaneously to expand the volume of the globular part of it. These two types of changes affect the modeling in a correlated way, with the result that good fits could be achieved irrespective of the exact position at which mass is removed and, consequently, this modeling procedure appears to lack the sensitivity to assess the position of the light chain.

DISCUSSION

Unlike hydrodynamic methods, solution x-ray scattering measurements allow the determination of structural parameters such as the radius of gyration R_g and the maximum length, D_{max} without any a priori geometrical model for the particle shape. D_{max} can therefore be readily compared with particle dimensions obtained from electron micrographs. We have performed an x-ray scattering study in solution of myosin head with and without the LC2 light chain. Our results show that D_{max} remains constant upon LC2 removal while R_g is significantly altered. As far as the D_{max} is concerned there was, since the pioneering x-ray scattering work of Mendelson (D_{max} = 120 Å, Mendelson et al., 1980), a marked discrepancy between x-ray scattering results and electron microscopy determinations (L_{max} = 190 ± 20 Å). Some plausible artefacts like non-uniform stain spreading in electron microscopy and lack of sensitivity of small angle x-ray scattering to thin portions of proteins were invoked at the time to explain this disagreement. However our results lead to D_{max} values very close to the electron microscopy determinations. In particular, Elliott and Offer (1978), working with intact rabbit skeletal myosin, find a length of 190 Å for the head and also derive, from the model they propose, an R_g value of 46.5 Å not inconsistent with our experimental determination on S1 (+LC2). This agreement between two so different methods, which can be plagued by entirely different artefacts such as those just mentioned, gives a very strong support to the common result.

S1 is known to be rather labile, probably as a consequence of its being a proteolytic fragment. Indeed, in our experiments, sensitivity to x-ray irradiation could be detected by comparison of successive scattering patterns after exposures as short as 10 min. This was also observed by high performance size exclusion chromatography analysis of samples immediately following x-ray exposure, which showed the presence of aggregated S1 (data not shown). Monodispersity can even be lost in the absence of x-ray irradiation: on one occasion, a problem with the storage ring caused a delay of 36 h between the final chromatography and the x-ray experiment. Data analysis showed a small but significant upward curvature in the Guinier plot (data not shown) indicative of the presence of a small amount of S1-aggregates. It is also worth noting that the angular region over which the Guinier plots are linear is fairly limited, especially in the case of S1 (+LC2) (see Fig. 2). At the large s end, the curve leaves the straight line on the upper side in the way characteristic of elongated particles to form a second, quasi linear section. The first data published on the myosin head barely reached the outer limit of the Guinier region, leading to a smaller value of the radius of gyration. All those factors probably contribute to account for the differences between our R_g and D_{max} determinations and previously published x-ray values (Mendelson et al., 1980). Recently, Mendelson and co-workers performed very interesting neutron scattering experiments on S1 myosin bound to actin filaments made "invisible" by deuteration (Curmi et al., 1988). Their objective was to compare the scattering pattern of bound S1 to that of free S1. Their data showed some upward curvature at low s that they ascribed to a combination of some S1 aggregation, residual actin scattering or some parasitic instrumental scattering. This is why they had to restrict themselves to the angular range 3.2×10^{-5} $Å^{-2} < s^2 < 6.0 \times 10^{-5}$ $Å^{-2}$ to derive what they called apparent radii of gyration. If one considers the data for both S1 fragments on Fig. 2 in the same angular range it appears that the roughly linear curves will yield underestimates for

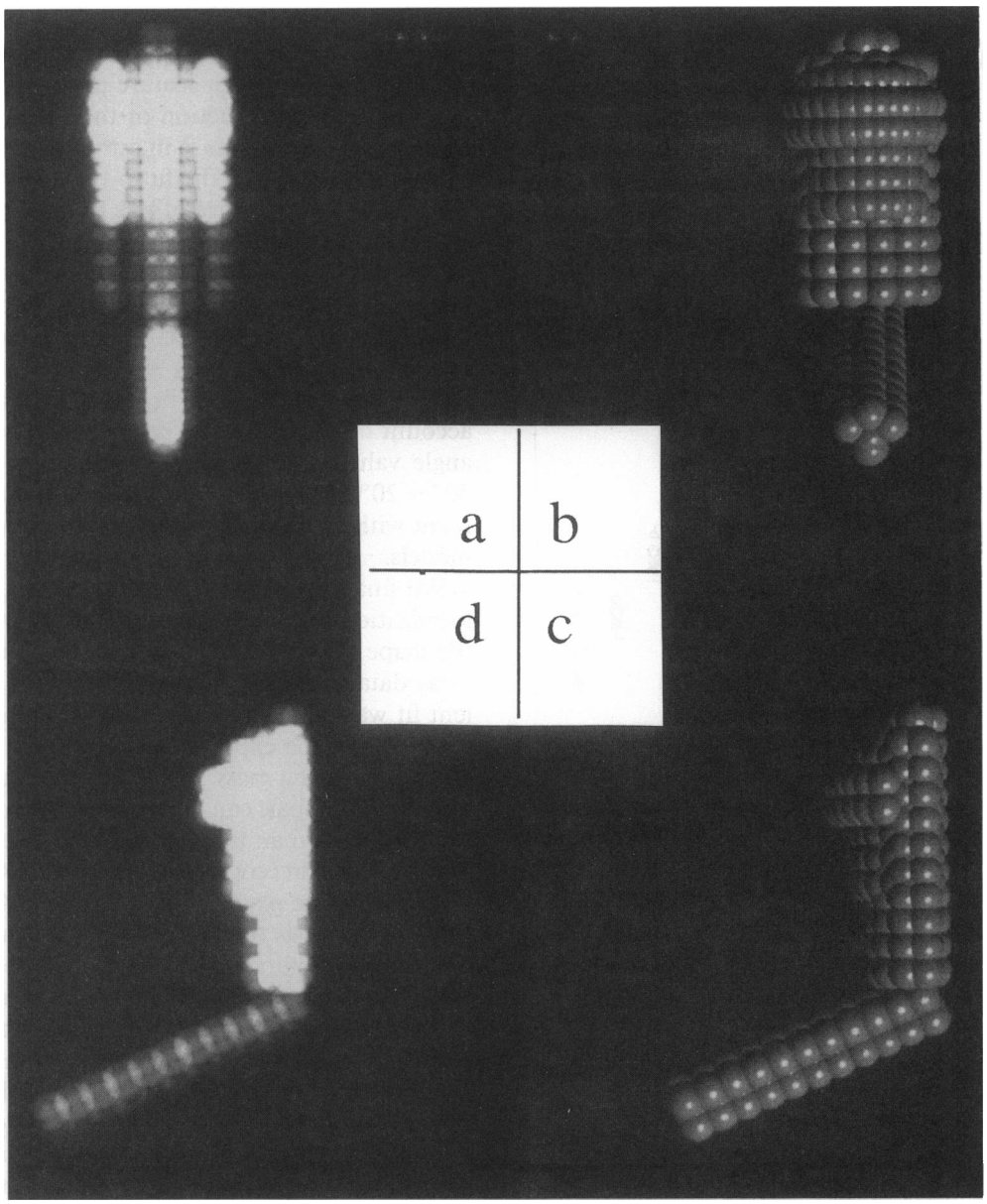

FIGURE 6 Model representations. Surface representation of two orthogonal views of the model for S1 (+LC2) (*b* and *c*) and their corresponding mass projections on the plane of view (*a* and *d*). Note that most of the mass is located at the globular portion of the head and the relatively low mass density at the tail end. The contour length of the model is 210 Å.

both R_g which moreover happen to be very close to one another. More recently, however, the same group managed to extend their neutron scattering experiments to smaller *s*-values and obtained R_g values close to ours (Mendelson et al., 1990).

The ratio of the radius of gyration of a particle to the third root of its molecular weight, $R_g/M_r^{1/3}$, can be taken as an index of its anisometry. For most globular proteins this ratio is in the range 0.6 to 0.75. Its value is 0.83 for S1 (−LC2) and reaches 0.92 for S1 (+LC2). This is indicative of a marked anisometry for both fragments, even larger in the case of S1 (+LC2), in agreement with most observations.

A more detailed shape can be proposed for the native myosin head on the basis of model calculations. The model shown in Fig. 6 is certainly not unique. However, it is clear that its main features must be present in any satisfactory model: the length to width ratio has to be between 4 and 5, supporting the view of a strongly anisometric particle, while most of the mass is located at one extremity to form an asymmetric globular part which tapers smoothly towards the thinner end (Fig. 6). The overall shape is very reminiscent of that deduced from electron micrographs (Elliott and Offer, 1978; Takahashi, 1978; Tokunaga et al., 1991; Winkelmann et al., 1991). Models for the general shape of the myosin head

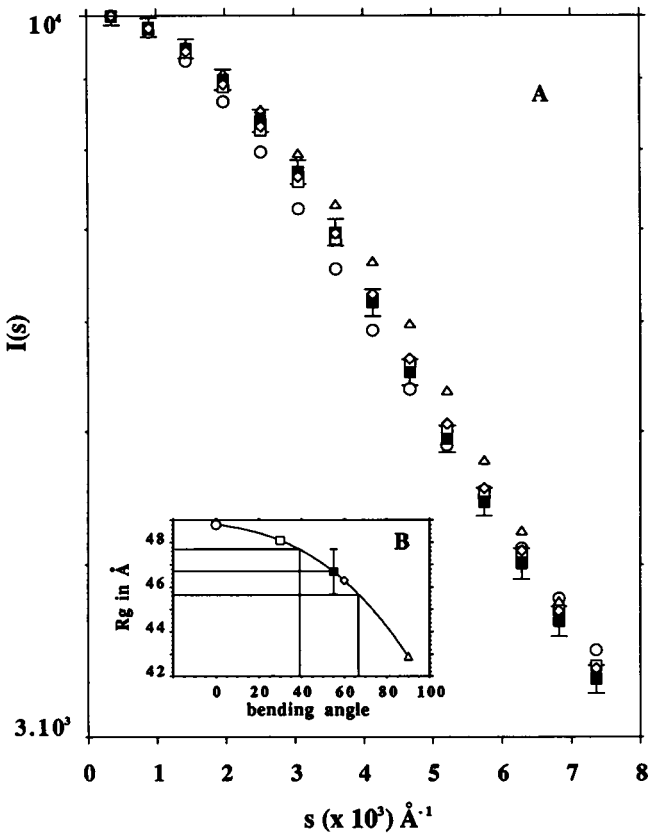

FIGURE 7 Comparison of calculated and experimental data for S1 (+LC2): the influence of the bending angle. (*A: filled squares*) Experimental points with associated error bars; (*open symbols*) calculated values corresponding to various values of the angle α between the globular part and the thinner end; (*open circles*) $\alpha = 0°$; (*open squares*) $\alpha = 30°$; (*open diamonds*) $\alpha = 60°$; (*open triangles*) $\alpha = 90°$. (*B*) Value of the radius of gyration vs. α. Symbols are used as in *A*.

have been proposed on the basis of three-dimensional image reconstructions of acto-myosin complexes. Some models suggest a rather globular shape with a D_{max} in the range 120–150 Å (Taylor and Amos, 1981; Amos et al., 1982). Others are more anisometric with a D_{max} in the range 160–190 Å (Moore et al., 1970; Toyoshima and Wakabayashi, 1985; Seymour and O'Brien, 1985; Milligan and Flicker, 1987; Kajiyama, 1988). Our results support the second class of models; in particular, our D_{max} value agrees with the contour length measured by Kajiyama (1988). Winkelmann and coll. recently derived a three-dimensional reconstruction of S1 (+LC2) from the analysis of a series of electron micrographs of thin-sectioned crystals (Winkelmann et al., 1991); the shape of their model shows most of the features observed in the consensus model derived from our SAXS data and would probably give a decent fit to our data with the likely exception of the Guinier region where its shorter size (contour length 165 Å, maximal chord 145 Å) would probably yield a smaller radius of gyration. However, this marked discrepancy in length should be seen in the context of the large uncertainty affecting their length determination as mentioned by the authors themselves.

Curvature is another feature present in most models from image reconstruction of the native myosin head. Introduction of curvature in our model lead to a significant improvement of the fit to the experimental curve, supporting the existence of this feature in solution. The localization of the bend was suggested by Botts et al. (1989) who applied a distance geometry program to distances derived from fluorescence resonance energy transfer mapping and electron microscopy. Thanks to the sensitivity of the very small angle region (Guinier region) to the value of the bending angle, and taking into account the experimental error bars, we clearly exclude angle values of 0° and 90° and derive an estimate of 50° ± 20° for this parameter. This is in qualitative agreement with the appearance of most electron microscopy models.

We finally attempted to address the question of the localization of LC2 and of the effect of LC2 removal on the shape of S1 by comparing models obtained from our x-ray data on S1 (+LC2) and S1 (−LC2). While excellent fit was obtained in the case of the native head, we could not fit the experimental curve for S1 (−LC2) by simply removing mass. The required volume expansion of the globular part can be performed in many directions which results in an undetermination of the localization of mass removal (corresponding to the LC2 light chain) provided it take place at one extremity. A large body of evidence suggests that LC2 is located near the head-rod junction. Structural analyses of actin decorated by S1, with or without LC2, exhibit mass differences at the caudal region of S1 (Craig et al., 1980; Vibert and Craig, 1982). Electron microscopic visualization with monoclonal antibody against LC2 has supported this localization (Winkelmann et al., 1983). The position of the NH_2-terminus of myosin LC2 of rabbit skeletal muscle was mapped on the myosin head with a monoclonal antibody which recognizes the amino acid sequence at the NH_2 terminus of LC2 and found to be located at the head-rod junction (Tokunaga et al., 1987). This is supported by the large decrease in the radius of gyration associated with LC2 removal. In conclusion, our results are consistent with the suggestion by Margossian and Slayter of an LC2 lying at a distance from the center of gravity (marked decrease in R_g) but going no further than one extremity of S1 (−LC2) (constant D_{max}).

Electron microscopy observations show that LC2 removal results in a loss of an elongated pear-shape to yield more rounded heads (Flicker et al., 1983; Winkelmann and Lowey, 1986; Margossian and Slayter, 1987; Walker and Trinick, 1989). In some studies, this change of shape is accompanied by a reduction in length (60 Å for Flicker et al., 1983; 26 Å for Walker and Trinick, 1989) while Margossian and Slayter (1987) do not detect any change in length. This last discrepancy might only be apparent since the density of mass at the thinner end is so

weak in projections as to make difficult the determination of the length of the head (Fig. 6, *b* and *d*). Our attempts at modeling S1 (−LC2), although unable to yield an unambiguous model, showed, beyond mass removal, a requirement for an expansion of the globular part of the molecule by up to 20% in order to achieve convergence with the experimental data. This suggests that the removal of the LC2 light chain may result in an increase flexibility and loosening of the structure.

Our results, which should contribute to clarify the question of S1 size, are being currently used for a detailed interpretation of recent muscle x-ray diffraction experiments performed at the SRS laboratory in Daresbury (J.B. and colleagues). Taking advantage of the recently determined structure of actin (Kabsch et al., 1990) combined with the present results, we have also undertaken an x-ray scattering study on nonpolymerizable actin-S1 complexes in solution using MBS-modified actin (Bettache et al., 1989).

Note added in proof: After this paper had been accepted, we became aware of two recent works on S1 (+LC2). The first one by Wakabayashi and colleagues (Photon Factory Annual Report, 1992), reports SAXS experiments on S1 (+LC2) in the presence and absence of various nucleotides. They report an R_g value of 47.8 Å (reduced to 45 Å in the presence of Mg-ATP) and a D_{max} of ~170 Å; both values are compatible with our results when uncertainties are taken into account. The high resolution structure of S1 (+LC2) has been reported in recent meetings (Winkelman et al., 1992; Tsukuba, 1992). The general shape of the protein is very similar to the result of the three-dimensional reconstruction proposed by Winkelman et al. (1991) and to the model presented here. Although the maximal chord is ~145 Å, this value might not be incompatible with the results from solution studies. Indeed, a small part of LC2, at one end of the molecule, is not visible in the crystal. Furthermore, the well documented flexibility of the molecule in solution might lead to a somewhat more extended conformation in solution (at least 170 Å) than in the crystal.

We are grateful to Dr. P. Tauc for his generous gift of ATCase. We thank D. Svergun for making available to us the latest version of his program GNOM. We thank the operators of the storage ring LURE-DCI and the staff of the computing center of LURE. We would like to thank Dr. E. Pantos and J. West of the computer division at Daresbury Laboratory for their help in the development of the programme DALAI and J. Harries at the Daresbury SRS for many discussions about the model fitting procedures.

Received for publication 21 February 1992 and in final form 20 July 1992.

REFERENCES

Amos, L. A., H. E. Huxley, K. C. Holmes, R. S. Goody, and K. A. Taylor. 1982. Structural evidence that myosin heads may interact with two sites on F-actin. *Nature (Lond.)*. 299:467–469.

Bettache, N., R. Bertrand, and R. Kassab. 1989. Coupling of nonpolymerizable monomeric actin to the F-actin binding region of the myosin head. *Proc. Natl. Acad. Sci. USA*. 86:6028–6032.

Bordas, J., M. H. J. Koch, P. N. Clout, E. Dorrington, C. Boulin, and A. Gabriel. 1980. A synchrotron radiation camera and data acquisition system for time-resolved x-ray scattering studies. *J. Phys. E. Sci. Instrum.* 13:938–944.

Botts, J., J. F. Thomason, and M. F. Morales. 1989. On the origin and transmission of force in actomyosin subfragment 1. *Proc. Natl. Acad. Sci. USA*. 86:2204–2208.

Craig, R. W., A. G. Szent-Györgyi, L. Beese, P. F. Flicker, P. J. Vibert, and C. Cohen. 1980. Electron microscopy of thin filaments decorated with a Ca^{2+}-regulated myosin. *J. Mol. Biol.* 140:35–55.

Craig, R., J. Trinick, and P. Knight. 1986. Discrepancies in length of myosin head. *Nature (Lond.)* 320:688.

Curmi, P. M. G., D. B. Stone, D. K. Schneider, J. A. Spudich, and R. A. Mendelson. 1988. Comparison of the structure of myosin subfragment-1 bound to actin and free in solution. A neutron scattering study using actin made "invisible" by deuteration. *J. Mol. Biol.* 203:781–798.

d'Albis, A., C. Pantaloni, and J-J. Béchet. 1979. An electrophoretic study of native myosin isozymes and of their subunit content. *Eur. J. Biochem.* 99:261–272.

Depautex, C., C. Desvignes, P. Leboucher, M. Lemonnier, D. Dagneaux, J. P. Benoit, and P. Vachette. 1987. The small-angle x-ray scattering instrument D24 *LURE Annual Report.*

Elliott, A., and G. Offer. 1978. Shape and flexibility of the myosin molecule. *J. Mol. Biol.* 123:505–519.

Flicker, P. F., T. Wallimann, and P. Vibert. 1983. Electron microscopy of scallop myosin. Location of regulatory light chains. *J. Mol. Biol.* 169:723–741.

Garrigos, M., and P. Vachette. 1989. Solution x-ray scattering studies of rabbit myosin subfragment-1. *Biophys. J.* 55:80*a*. (Abstr.)

Glatter, O. 1977. A new method for the evaluation of small-angle scattering data. *J. Appl. Cryst.* 10:415–421.

Guinier, A., and G. Fournet. 1955. Small-Angle Scattering of X-rays. John Wiley and Sons, New York.

Hoover, T. A., W. D. Roof, K. F. Foltermann, G. A. O'Donovan, D. A. Bencini, and J. R. Wild. 1983. Nucleotide sequence of the structural gene (pyrB) that encodes the catalytic polypeptide of aspartate transcarbamoylase of Escherichia coli. *Proc. Natl. Acad. Sci. USA*. 80:2462–2466.

Kabsch, W., H. G. Mannherz, D. Suck, E. F. Pai, and K. C. Holmes. 1990. Atomic structure of the actin: DNaseI complex. *Nature (Lond.)*. 347:37–44.

Kajiyama, H. 1988. Shape of the myosin head in the rigor complex. Three-dimensional image reconstruction of the actin-tropomyosin-heavy meromyosin complex. *J. Mol. Biol.* 204:639–652.

Knight, P., and J. Trinick. 1984. Structure of the myosin projections on native thick filaments from vertebrate skeletal muscle. *J. Mol. Biol.* 177:461–482.

Luzzati, V. 1960. Interprétation des mesures absolues de diffusion centrale des rayons-X en collimation ponctuelle et linéaire: solutions de particules globulaires et de bâtonnets. *Acta Crystallogr.* 13:939–945.

Margossian, S. S., and S. Lowey. 1982. Preparation of myosin and its subfragments from rabbit skeletal muscle. *Methods Enzymol.* 85:55–71.

Margossian, S. S., and H. S. Slayter. 1987. Electron microscopy of cardiac myosin: its shape and properties as determined by the regulatory light chain. *J. Muscle Res. Cell Motil.* 8:437–447.

Mendelson, R., and K. M. Kretzschmar. 1980. Structure of myosin subfragment 1 from low-angle x-ray scattering. *Biochemistry.* 19:4103–4108.

Mendelson, R., P. Curmi, D. Schneider, and D. Stone. 1990. Radius of gyration of myosin S1 when free and when bound to F-Actin. *Biophys. J.* 57:544*a*. (Abstr.)

Milligan, R. A., and P. F. Flicker. 1987. Structural relationships of actin, myosin, and tropomyosin revealed by cryo-electron microscopy. *J. Cell Biol.* 105:29–39.

Moody, M. F., P. Vachette, and A. M. Foote. 1979. Changes in the

x-ray solution scattering of aspartate transcarbamylase following the allosteric transition. *J. Mol. Biol.* 133:517–532.

Moore, P. B., H. E. Huxley, and D. J. DeRosier. 1970. Three-dimensional reconstruction of F-actin, thin filaments and decorated thin filaments. *J. Mol. Biol.* 50:279–295.

Perry, S. V. 1955. Myosin adenosinetriphosphatase. Enzymes in phosphate metabolism. *Methods Enzymol.* 2:582–588.

Seymour, J., and E. J. O'Brien. 1985. Structure of myosin decorated actin filaments and natural thin filaments. *J. Muscle Res. Cell Motil.* 6:725–756.

Slayter, H. S., and S. Lowey. 1967. Substructure of the myosin molecule as visualized by electron microscopy. *Proc. Natl. Acad. Sci. USA.* 58:1611–1618.

Squire, J. 1981. The Structural Basis of Muscular Contraction. Plenum Press, New York. 318–329.

Squire, J., and P. J. Vibert, editors. 1987. Fibrous Protein Structure. Academic Press, London. 283–306.

Svergun, D. I., A. V. Semenyuk, and L. A. Feigin. 1988. Small-angle scattering data treatment by the regularization method. *Acta Cryst.* A44:244–251.

Takahashi, K. 1978. Topography of the myosin molecule as visualized by an improved negative staining method. *J. Biochem.* 83:905–908.

Taylor, K. A., and L. Amos. 1981. A new model for the geometry of the binding of myosin crossbridges to muscle thin filaments. *J. Mol. Biol.* 147:297–324.

Tokunaga, M., M. Suzuki, K. Saeki, and T. Wakabayashi. 1987. Location of the ATPase site of myosin determined by three-dimensional electron microscopy. *J. Mol. Biol.* 194:245–255.

Tokunaga, M., K. Sutoh, and T. Wakabayashi. 1991. Structure and structural change of the myosin head. *Adv. Biophys.* 27:157–167.

Tong, S. W., and M. Elzinga. 1990. Amino-acid sequence of rabbit skeletal muscle myosin. 50-kDa fragment of the heavy chain. *J. Biol. Chem.* 265:4893–4901.

Toyoshima, C., and T. Wakabayashi. 1985. Three-dimensional image analysis of thin filaments and myosin molecules from skeletal muscle. IV. Reconstruction from minimal- and high-dose images of the actin-tropomyosin-myosin subfragment-1 complex. *J. Biochem.* 97:219–243.

Toyoshima, Y. Y., S. J. Kron, E. M. McNally, K. R. Niebling, C. Toyoshima, and J. A. Spudich. 1987. Myosin subfragment-1 is sufficient to move actin filaments in vitro. *Nature (Lond.).* 328:536–539.

Vibert, P. 1988. Domain structure of the myosin head in correlation-averaged images of shadowed molecules. *J. Muscle Res. Cell Motil.* 9:147–155.

Vibert, P., and R. Craig. 1982. Three-dimensional reconstitution of thin filaments decorated with a Ca^{2+}-regulated myosin. *J. Mol. Biol.* 157:299–319.

Walker, M., P. Knight, and J. Trinick. 1985. Negative staining of myosin molecules. *J. Mol. Biol.* 184:535–542.

Walker, M., and J. Trinick. 1989. Electron microscopy of negatively stained scallop myosin molecules. Effect of regulatory light chain removal on head structure. *J. Mol. Biol.* 208:469–475.

Winkelmann, D. A., S. Lowey, and J. L. Press. 1983. Monoclonal antibodies localize changes on myosin heavy chain isozymes during avian myogenesis. *Cell.* 34:295–306.

Winkelmann, D. A., H. Mekeel, and I. Rayment. 1985. Packing analysis of crystalline myosin subfragment-1. Implications for the size and shape of the myosin head. *J. Mol. Biol.* 181:487–501.

Winkelmann, D. A., and S. Lowey. 1986. Probing myosin head structure with monoclonal antibodies. *J. Mol. Biol.* 188:595–612.

Winkelmann, D. A., T. S. Baker, and I. Rayment. 1991. Three-dimensional structure of myosin subfragment-1 from electron microscopy of sectioned crystals. *J. Cell Biol.* 114:701–713.